Earth and Planetary Science Letters 511 (2019) 67–75

Contents lists available at ScienceDirect

Earth and Planetary Science Letters

www.elsevier.com/locate/epsl

New constraints on mantle carbon from Mid-Atlantic Ridge popping rocks

M.R. Jones [a,*], V.D. Wanless [b], S.A. Soule [c], M.D. Kurz [c], E. Mittelstaedt [d], D.J. Fornari [c], J. Curtice [c], F. Klein [c], V. Le Roux [c], H. Brodsky [e], S. Péron [f], D.M. Schwartz [b]

[a] Massachusetts Institute of Technology/Woods Hole Oceanographic Institution Joint Program in Oceanography, 360 Woods Hole Road, 02543, Woods Hole, MA, USA
[b] Department of Geosciences, Boise State University, 83725, Boise, ID, USA
[c] Department of Geology and Geophysics, Woods Hole Oceanographic Institution, 02543, Woods Hole, MA, USA
[d] Department of Geological Sciences, University of Idaho, 83844, Moscow, ID, USA
[e] Department of Mechanical and Industrial Engineering, Northeastern University, 02115, Boston, MA, USA
[f] Institut de Physique du Globe de Paris – Sorbonne Paris Cité, UMR CNRS 7154, Université Paris Diderot, 1 Rue Jussieu, 75005, Paris, France

ARTICLE INFO

Article history:
Received 2 August 2018
Received in revised form 7 January 2019
Accepted 10 January 2019
Available online 4 February 2019
Editor: T.A. Mather

Keywords:
carbon
mid-ocean ridge basalts
mantle
popping rocks
volatiles
vesicularity

ABSTRACT

Despite the influence of mantle carbon on melt formation and migration, global volatile budgets, and volcanic eruption styles, the carbon concentration in Earth's upper mantle remains highly debated, with estimates varying by more than an order of magnitude. The relationship between carbon and incompatible trace element (e.g., Nb, Ba) concentrations in rare, undegassed mid-ocean ridge basalts and melt inclusions provide primary constraints on upper mantle carbon content. Here we investigate whether the most volatile rich mid-ocean ridge basalts, termed 'popping rocks', represent undegassed magmas from the upper mantle and provide insight into upper mantle carbon inventory. We show that fourteen new popping rocks, collected *in situ* from the Mid-Atlantic Ridge rift valley near 14°N, contain highly variable CO_2/Nb and CO_2/Ba ratios despite similar mantle sources and extents of melting. We revise the original model for popping rock formation using seafloor observations, high-resolution bathymetry, vesicle size distributions, major and trace element geochemistry, and noble gas geochemistry. Highly variable volatile concentrations despite relatively homogeneous trace element ratios and low $^4He/^{40}Ar^*$ suggest that bubble accumulation affected these popping rocks. These results provide evidence for heterogeneity in the CO_2/Ba ratio of the depleted mantle and indicate that mantle carbon concentrations are lower and less heterogeneous than previously estimated, which influences models for mantle melting and CO_2 flux at mid-ocean ridges.

1. Introduction

Volatiles in Earth's mantle strongly impact melt formation and migration (Dasgupta and Hirschmann, 2010), geophysical properties of the Earth's interior (Hirth and Kohlstedt, 1996), the behavior of volcanic eruptions (Wallace et al., 2015), and long-term atmospheric evolution (Huybers and Langmuir, 2009). Thus, knowledge of volatile species in the upper mantle is crucial to understanding Earth's formation and evolution. However, shallow degassing makes estimating pre-eruptive magmatic volatile concentrations notoriously difficult, resulting in several decades of debate about the carbon concentration of the upper mantle (Burnard et al., 2014; Cartigny et al., 2008; Chavrit et al., 2014; Dasgupta et al., 2013; Javoy and Pineau, 1991; Le Voyer et al., 2017; Marty and Tolstikhin, 1998; Michael and Graham, 2015; Rosenthal et al., 2015; Saal et al., 2002). The most common approach for estimating upper mantle carbon content and mid-ocean ridge (MOR) CO_2 flux relies on incompatible elements that behave in a similar manner to carbon during melting and crystallization, such as Nb or Ba, and inferences about these ratios from rare, undegassed melts. Volatile undersaturated olivine-hosted melt inclusions from the Siqueiros Transform Fault (Saal et al., 2002) and global ultra-depleted MOR basalts (MORB) (Michael and Graham, 2015) yield average CO_2/Nb ratios of 239–283 (Fig. 1), corresponding to an average mantle source CO_2 concentration of 72–85 ppm. In contrast, undegassed melt inclusions (Le Voyer et al., 2017) from the Mid-Atlantic Ridge (MAR) yield much higher CO_2/Nb ratios of 556–557 (Fig. 1). One recent study suggested that the difference between these estimates for undegassed CO_2/Nb reflects heterogeneity in upper mantle ratios, implying that mantle carbon con-

* Corresponding author.
E-mail address: meghanj@mit.edu (M.R. Jones).

https://doi.org/10.1016/j.epsl.2019.01.019
0012-821X/

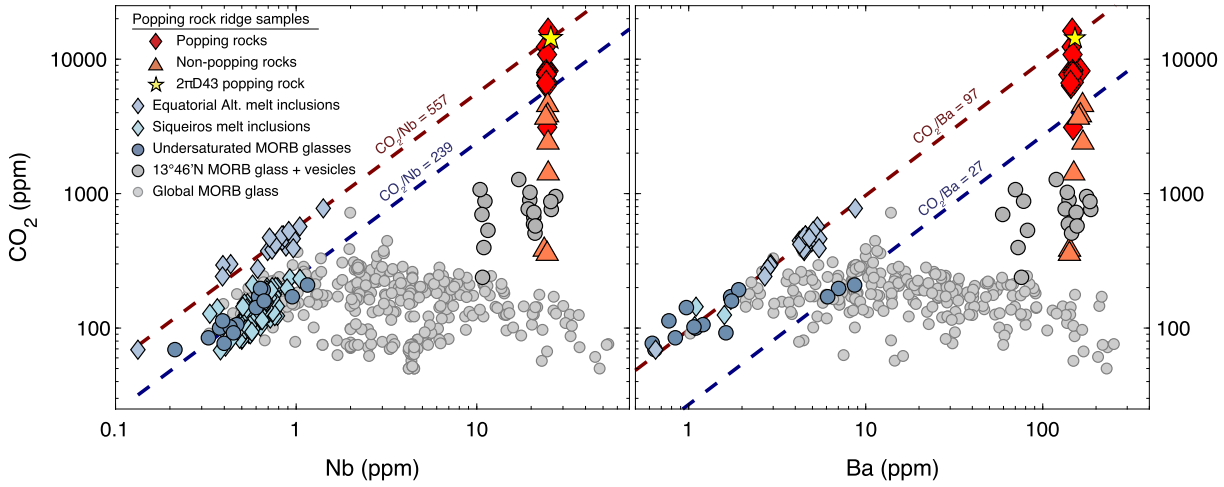

Fig. 1. Variation in CO_2 concentration as a function of Nb and Ba concentration. Red diamonds represent the fourteen new popping rocks collected from the Mid-Atlantic Ridge near 13°46′N while orange triangles represent proximal non-popping rocks with indistinguishable REE patterns and trace elements ratios. CO_2 concentrations presented in this study were reconstructed from the dissolved concentrations, vesicularity, and measured CO_2 density within bubbles. Data sources: 2πD43 popping rock: Sarda and Graham (1990), Bougault et al. (1988), and Cartigny et al. (2008); Equatorial Atlantic melt inclusions: Le Voyer et al. (2017); Siqueiros melt inclusions: Saal et al. (2002); Undersaturated MORB glasses: Michael and Graham (2015); global MORB glass compilation from PetDB. (For interpretation of the colors in the figure(s), the reader is referred to the web version of this article.)

tent varies by nearly two orders of magnitude when combined with estimated depleted MORB mantle (DMM) Nb concentrations (Le Voyer et al., 2017). Another study proposed that differences in these ratios reflects partial degassing and magma mixing, implying constant CO_2/incompatible trace element ratios and less heterogeneity in mantle carbon abundances (Matthews et al., 2017). Additional observational constraints are essential for establishing the abundance and heterogeneity of carbon in Earth's mantle.

The only volatile saturated MORB that has been used to directly constrain mantle volatile concentrations was dredged in 1985 near 14°N on the MAR by the *R/V Akademik Boris Petrov* (Bougault et al., 1988). Upon recovery, the dredged '2πD43' samples began popping on the ship's deck due to their removal from seafloor pressures and the consequential release of trapped volatiles from vesicles. Due to their high volatile abundances, simple vesicle size distributions, and unique rare gas ratios, the 2πD43 popping rocks have been interpreted as the most representative samples of undegassed magmas sourced from the upper mantle (Burnard, 1997; Cartigny et al., 2008; Javoy and Pineau, 1991; Moreira et al., 1998; Sarda and Graham, 1990). The CO_2 and incompatible trace element concentrations in the 2πD43 samples are enriched relative to undegassed, undersaturated MORB and melt inclusions, and thus provide a unique constraint on these ratios and potentially mantle carbon concentrations (Fig. 1). However, the lack of geologic context for these samples, recovered by dredging on poorly mapped seafloor, has prompted debate about their origins and the implications for mantle carbon (Cartigny et al., 2008; Chavrit et al., 2014; Le Voyer et al., 2017; Sarda and Graham, 1990). Here, we report the CO_2 concentrations, geochemistry, vesicle size distributions, and geologic setting for fourteen new popping rock samples collected from the same ridge segment as dredge 2πD43 during a 2016 *R/V Atlantis* cruise (AT33-03). Our results provide new constraints on the formation of popping rocks and yield insight into heterogeneities in mantle carbon concentrations and eruptive processes at magma-poor ridge segments.

2. Methods

2.1. Major and trace elements

Major element concentrations were measured using the Cameca SXFive electron microprobe at Boise State University. Sample preparation techniques are described in Schwartz et al. (2017). Analyses were conducted using an accelerating voltage of 15 kV, a beam current of 10 nA, and a beam diameter of 10 µm. Al, K, and Mg were measured for 50 s, Si and Ca were measured for 40 s, Ti, Na, Fe, and P were counted for 30 s, and Mn was counted for 20 s. Five spots were measured on glass chips and averaged. Basalt standard VG-2s and internal standard 2392-9 (Perfit et al., 2012) were run approximately every 5 samples to account for instrument drift. Repeat analyses of standard glasses indicate that the analytical precision of most major elements is <1% to 3%, with the exception of MnO and P_2O_5, which have higher relative errors (5–25%) due to low concentrations.

Trace element concentrations were determined using a Thermo-Electron X-Series II Quadrupole Inductively Coupled Plasma Mass Spectrometer (ICP-MS) at Boise State University. Samples were dissolved and analyzed following methods outlined in Schwartz et al. (2017). Each solution was measured three times; averages and standard deviations are provided in Supplementary Table 1. Standards were measured before and after each run and standard JB-3 was analyzed approximately every 10 samples to account for instrument drift.

2.2. Volatile elements

Volatile (H_2O, CO_2, S, F, and Cl) analyses were carried out at the Northeast National Ion Microprobe Facility (NENIMF) at the Woods Hole Oceanographic Institution (WHOI) using high mass resolution secondary ion mass spectrometry (CAMECA IMS 1280), using sample preparation and measurement techniques developed by Hauri et al. (2002) and described in Schwartz et al. (2017). Each sample was measured multiple times; averages are provided in Supplementary Table 2. Calibration curves were established using nine standard glasses and drift was assessed using repeat measurements on standard glass ALV519-4-1 (Hauri et al., 2002). Analytical uncertainty ($2\sigma \sim 10\%$) has been established for these procedures at NENIMF based on repeat measurements on standard glass 519-4-1.

2.3. Noble gas abundances and ratios

Helium, neon, and argon abundances and isotope compositions were analyzed using a MAP 215-50 mass spectrometer in the WHOI Isotope Geochemistry Facility, as described by

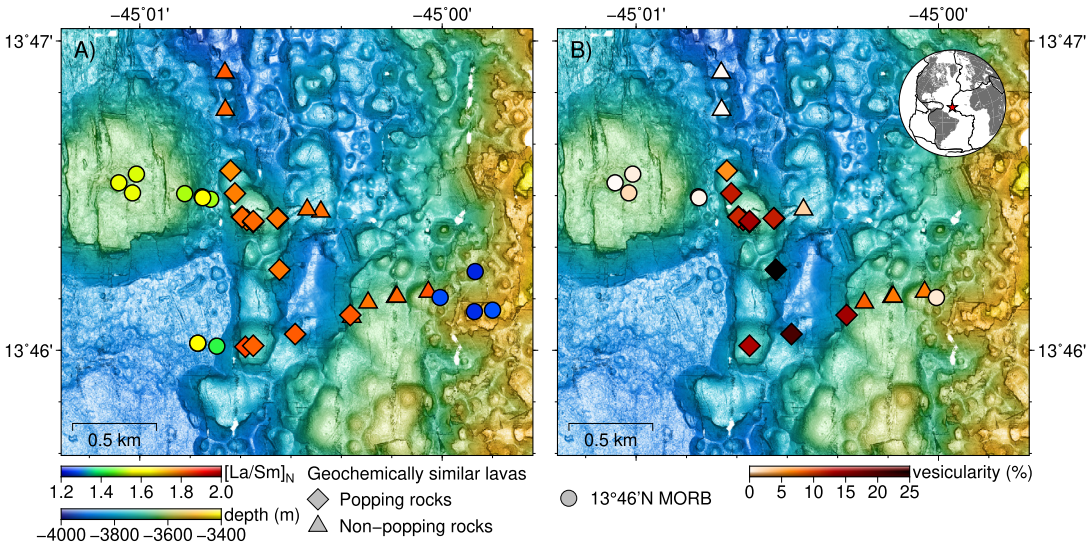

Fig. 2. 1 m resolution bathymetric maps showing the distribution of newly recovered popping rocks (diamonds). The bathymetry reveals that popping rocks are primarily restricted to a north–south trending pillow ridge and proximal pillow mounds. (A) Symbols are colored by $[La/Sm]_N$. (B) Symbols are colored by vesicularity. Despite relatively homogeneous trace element ratios, the vesicularity and total CO_2 concentrations in popping rocks varies dramatically (5–24 vol.% vesicles; 3,100–16,200 ppm CO_2). Several proximal, non-popping rocks (triangles) are geochemically similar to popping rocks but have notably lower vesicularities (<1–8 vol.% vesicles; 360–4,550 ppm CO_2). Inset map shows the location of the popping rocks on the Mid-Atlantic Ridge as a red star.

Kurz et al. (2005). The helium standard has a $^3He/^4He$ ratio of 8.35 times atmospheric (Ra) and is typically 5×10^{-9} cc STP ^4He. Air was used as the neon and argon standard ($\sim1.5 \times 10^{-10}$ cc STP neon and 9×10^{-8} cc STP argon). Noble gases are purified using three different SAES getters, operated between room temperature and 600 °C, and separated with two cryogenic cold traps (one charcoal and one stainless-steel "nude" trap). Crushing blanks are typically 1×10^{-11} cm^3 STP ^4He and 2×10^{-12} cm^3 STP ^{20}Ne and are insignificant relative to the gas quantities measured. Argon isotopes were measured using a dedicated Quadrupole Mass Spectrometer (Hiden). All measurements were made by crushing in vacuo, using well established procedures (e.g. Kurz et al., 2009). The quantities of gas introduced into the extraction line and mass spectrometers were controlled by capacitance manometry, followed by a pre-measurement with a quadrupole mass spectrometer and volumetric splitting prior to inlet to the mass spectrometer.

2.4. Vesicularity, vesicle size distributions, and exsolved volatile concentrations

X-ray computed microtomography (μ-CT) scans were collected using a table-top Bruker Skyscan 1272 at the Woods Hole Oceanographic Institution. Transmitted radiographs were collected at steps ranging from 0.15° to 0.35° over 180°. The source voltage ranged between 80 and 100 kV with a current between 100 and 125 μA. Filters and exposure times were selected based on the intensity of the transmitted x-rays, which principally varied based on sample size. The pixel resolution ranged between 3.4 and 5.0 μm. The scans were reconstructed using Bruker NRecon software with corrections applied for beam hardening, ring artifacts, and thermal misalignment. The 3D dataset was segmented using a global threshold in Bruker CTAn software. Cracks and non-vesicles were identified using Bruker visualization software and manually removed using ImageJ. Vesicularity and individual vesicle parameters were calculated using a combination of CTAn, ImageJ, and MATLAB image processing tools. Only vesicles larger than 15 μm in radius (~3× the minimum pixel resolution) were considered. Additional vesicularity measurements were acquired on 10× magnification reflected light photomicrographs of polished glass fragments from the outer quenched rind of the lava samples. The vesicularity measurements based on 2D and 3D techniques are similar; small differences likely reflect a combination of measurement uncertainties and natural variability between fragments.

The exsolved CO_2 concentrations were calculated from the vesicularity and average measured density of CO_2 in the vesicles. The density of CO_2 in the vesicles was determined at the Woods Hole Oceanographic Institution using a Horiba LabRam HR Raman spectrometer with a focal length of 800 mm. The instrument is equipped with a thermoelectrically cooled (−70 °C) Synapse® 1024 × 256 pixel open electrode CCD detector. Measurements were conducted following previously established protocols (Aster et al., 2016; Esposito et al., 2011; Lamadrid et al., 2017; Moore et al., 2015). All analyses were conducted with a 100× long working distance objective with a numerical aperture (NA) of 0.8 and a confocal hole diameter set to 300 μm. We used a 632 nm laser, a grating with 1800 grooves per mm, and a slit size of 30 μm. Spectra were collected for five 30 s accumulations between 1160 and 1429 cm^{-1}. The background for each sample was corrected for noise in LabSpec6 and the peaks were fit using a Gaussian function in MATLAB. The CO_2 Fermi diad splits were calibrated using the measured separation between the 1249.03 cm^{-1} and 1388.25 cm^{-1} bands for argon, using spectra collected at the beginning and end of the session. The measured separations between argon bands drifted by <0.05 cm^{-1}. The density of CO_2 within the vesicles was calculated based on the difference in wavenumber between the two peaks of the Fermi diad (Wright and Wang, 1973) according to the calibration developed by Lamadrid et al. (2017) at Virginia Tech for similar acquisition parameters (632 nm laser; 1800 grooves/mm grating). The variability between the density measurements provides an estimate of the uncertainties associated with this method of reconstructing total CO_2 concentrations (standard error is 0.01 g/cm^3).

3. Results

Fourteen new popping rocks were recovered *in situ* from the MAR axial valley at the 2πD43 dredge site, ~7 km west of the hanging-wall cutoff for the 13°48′N oceanic core complex (Fig. 2). These samples, as well as 43 non-popping rocks recovered within the rift valley near 13°46′N, were analyzed for major and trace

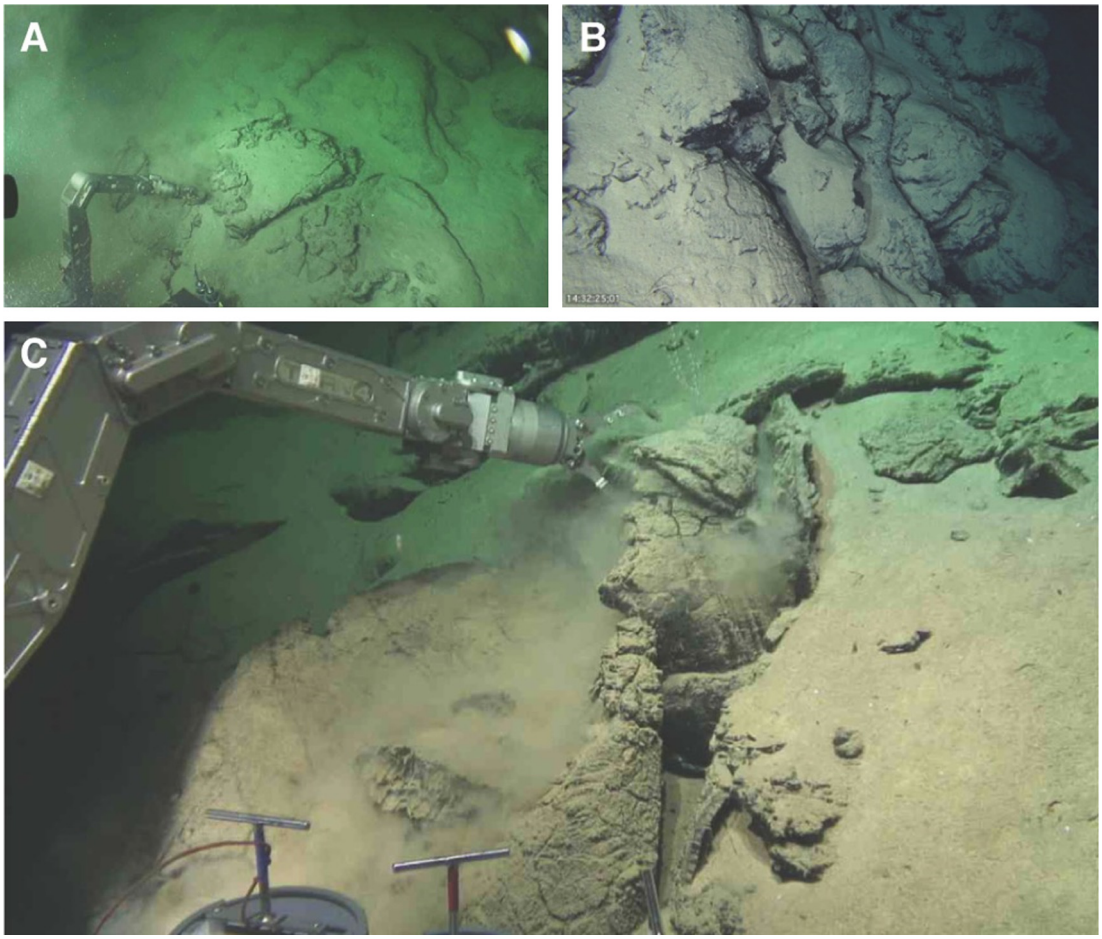

Fig. 3. Seafloor observations from Alvin dives AL4818 and AL4821, which traversed Popping Rock Ridge. (A) Popping rock AL4818-003, the first recovered *in situ*, collected from a sedimented, collapsed pillow lava. (B) Elongated pillows from the northern edge of Popping Rock Ridge. (C) Popping rock AL4821-057, collected from the outer crust of a collapsed pillow basalt.

elements and volatile concentrations (Supplementary Tables 1–2). Three popping rocks and three proximal, non-popping samples were analyzed for helium and argon abundances and isotopic compositions (Supplementary Table 3). *AUV Sentry* near-bottom multibeam bathymetry and *HOV Alvin* sampling and seafloor observations reveal that the popping rocks are primarily restricted to a north–south trending, heavily sedimented pillow ridge and proximal pillow mounds, which we refer to as 'Popping Rock Ridge' (Fig. 2; seafloor observations in Fig. 3). The popping rocks are remarkably homogeneous in major and trace element concentrations and ratios (e.g., $[La/Sm]_N = 1.76–1.84$; Fig. 2; Fig. 4), indicating similar mantle sources and extents of melting. The trace element ratios and rare earth element (REE) patterns in popping rocks are indistinguishable from eight proximal basalt samples that were not identified as popping rocks on the ship, many of which have notably lower vesicularities (Fig. 2; Fig. 4). The popping rocks (diamonds in Fig. 2) and eight proximal, non-popping rocks with similar REE patterns (triangles in Fig. 2) are geochemically distinct from all other lavas recovered from the region based on major and trace element compositions (circles in Fig. 2; Fig. 4; Supplementary Table 1).

The dissolved volatile concentrations (CO_2, H_2O, Cl, F, S) in the popping and non-popping samples are within the range commonly observed in MORB (Wallace et al., 2015; Supplementary Table 2). In contrast, the exsolved volatile concentrations in these popping rocks are amongst the highest ever recorded for submarine MORB, especially those outside the influence of mantle plumes (Chavrit et al., 2014; Supplementary Table 2). The vesicularity in the popping rocks ranges from 5–24 vol.% based on reflected light photomicrographs and x-ray micro-computed tomography scans (Figs. 5–6, Table 1). Based on the measured vesicularity, measured dissolved CO_2 concentrations, and the average CO_2 density within vesicles measured by Raman spectroscopy (Supplementary Table 4), the CO_2 concentration in these popping rocks varies from 3,100–16,200 ppm, where ppm is μg/g (Fig. 1; Table 1; Supplementary Table 2). The eight non-popping rocks that are geochemically similar overlap this range in vesicularity and total CO_2 concentration, but are on average lower (0.18–8.24 vol.%; 360–4,550 ppm CO_2; Figs. 1–2). We rely on the CO_2 concentrations estimated from vesicularity rather than measured by capacitance manometry during crushing for helium and argon analyses because the latter method does not account for gas loss through cracks prior to analysis.

The vesicle size distributions of moderate vesicularity samples (Fig. 5a–c) are distinct relative to high vesicularity popping rocks (Fig. 5d–f). Moderate vesicularity popping rocks (i.e., 5–7 vol.%) display simple log–linear vesicle size distributions (Fig. 5; Fig. 6). The vesicle size distributions of higher vesicularity samples deviate from log–linear relationships, with more abundant large vesicles (>1.5 mm diameter) than expected based on a simple continuous bubble nucleation and growth model (Cashman and Mangan, 1994) (Fig. 5; Fig. 6). The new popping rocks exhibit relatively homogeneous $^4He/^{40}Ar^*$ (1.05–1.09), where $^{40}Ar^*$ is the ^{40}Ar concentration corrected for atmospheric contamination ($^{40}Ar^* = {}^{36}Ar_{sample}$ ($^{40}Ar/^{36}Ar_{sample} - {}^{40}Ar/^{36}Ar_{air}$); e.g., Sarda and Moreira, 2002). The $^4He/^{40}Ar^*$ in three popping rocks and one geochemically similar, non-popping rock are slightly lower than the putative mantle

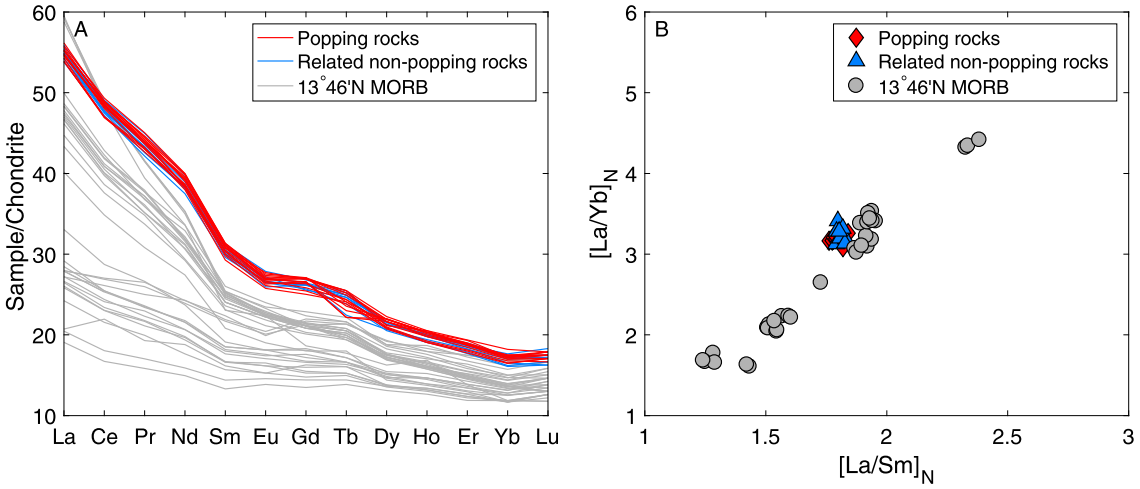

Fig. 4. (A) Rare earth element diagrams and (B) La/Yb vs. La/Sm comparing popping rocks (red; diamonds in Fig. 2), geochemically similar non-popping rocks (blue; triangles in Fig. 2), and geochemically distinct samples at 13°46′N (grey; circles in Fig. 2). Elements are normalized to CI carbonaceous chondrites (McDonough and Sun, 1995).

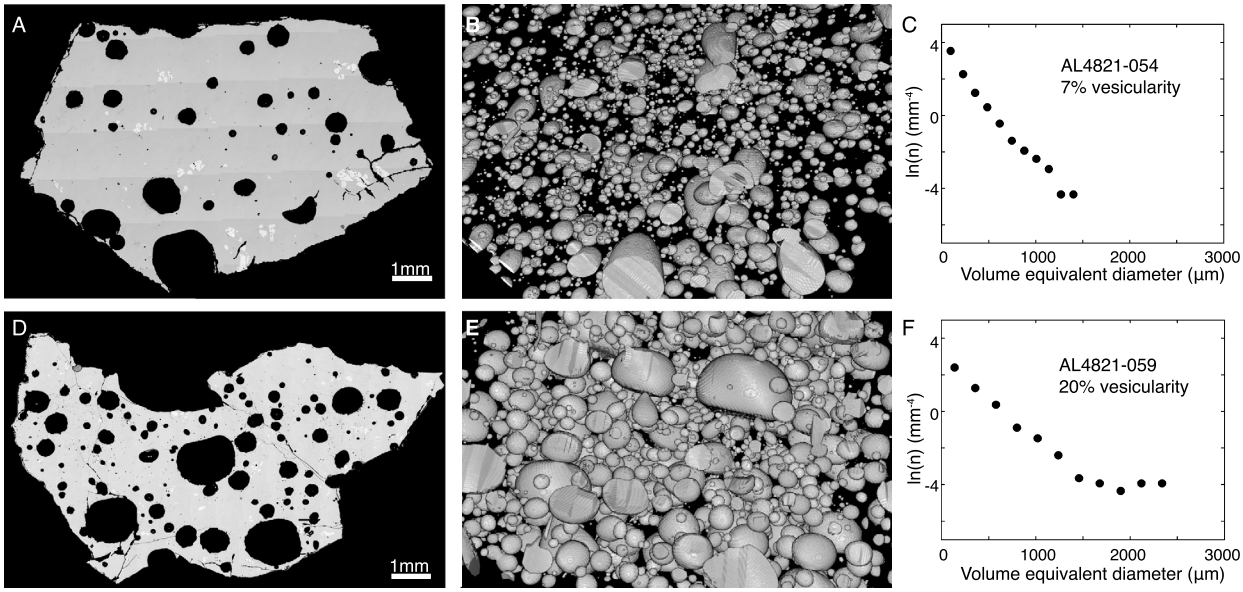

Fig. 5. Polished section images (A), (D), x-ray micro-computed tomography scans (B), (E), and vesicle size distributions based on x-ray μ-CT scans (C), (F) for an intermediate vesicularity (AL4821-054; top) and high vesicularity (AL4821-059; bottom) popping rock. The high vesicularity popping rocks show deviations from a simple log–linear vesicle size distribution at the largest size classes, likely due to bubble coalescence and/or accumulation.

production ratio of 3 ± 1 (Marty and Tolstikhin, 1998), while proximal, geochemically distinct non-popping samples exhibit elevated $^4He/^{40}Ar^*$ consistent with estimates for degassed MORB (Tucker et al., 2018) (Fig. 7). The popping rocks display $^3He/^4He$ ratios of 8.07–8.30 R_A and $CO_2/^3He$ ratios of 2.97 × 10^9–3.11 × 10^9. Proximal, non-popping rocks have $^3He/^4He$ ratios of 7.63–8.33 R_A and $CO_2/^3He$ ratios of 1.79 × 10^9–2.53 × 10^9.

4. Discussion

4.1. Origin of the high volatile concentrations in popping rocks

The most striking and novel observation from this study is that the new popping rock lavas display highly variable total CO_2 concentrations despite similar geochemistry and eruptive morphology (Table 1; Figs. 1–4). The similar trace element ratios and REE patterns in the fourteen newly recovered popping rocks and eight proximal non-popping samples (Fig. 2; Fig. 4) indicate that these lavas erupted from geochemically similar mantle sources, possibly during a series of closely timed eruptions based on their restricted

Table 1
Nb, Ba, vesicularity (3D and 2D), and total CO_2 concentrations (based on dissolved CO_2 concentrations, 2D vesicularity measurements, and the average CO_2 density in bubbles) for newly recovered in situ popping rocks. Uncertainties are detailed in the methods and supplementary material.

Sample	Nb (ppm)	Ba (ppm)	Ves. (3D) (%)	Ves. (2D) (%)	Total CO_2 (ppm)
AL4818-003	24.34	149.61	13.6	13.3	7633
AL4820-035	24.05	141.06			
AL4820-036	24.21	139.43	13.2	13.3	7663
AL4820-037	24.16	145.61	19.7	20.0	12368
AL4820-039	24.98	163.49		14.1	8178
AL4821-050	24.53	148.37	5.2	5.7	3112
AL4821-051	24.65	149.88	9.1	11.9	6731
AL4821-053	24.41	149.18	12.9	14.2	8270
AL4821-054	24.37	144.38	7.1	11.2	6345
AL4821-055	24.49	147.36	15.6	17.9	10823
AL4821-056	24.20	147.24	12.8	13.8	7993
AL4821-057	24.38	148.27	9.8	13.4	7731
AL4821-058	24.21	143.32	11.3	11.7	6643
AL4821-059	24.80	146.70	20.1	24.8	16231

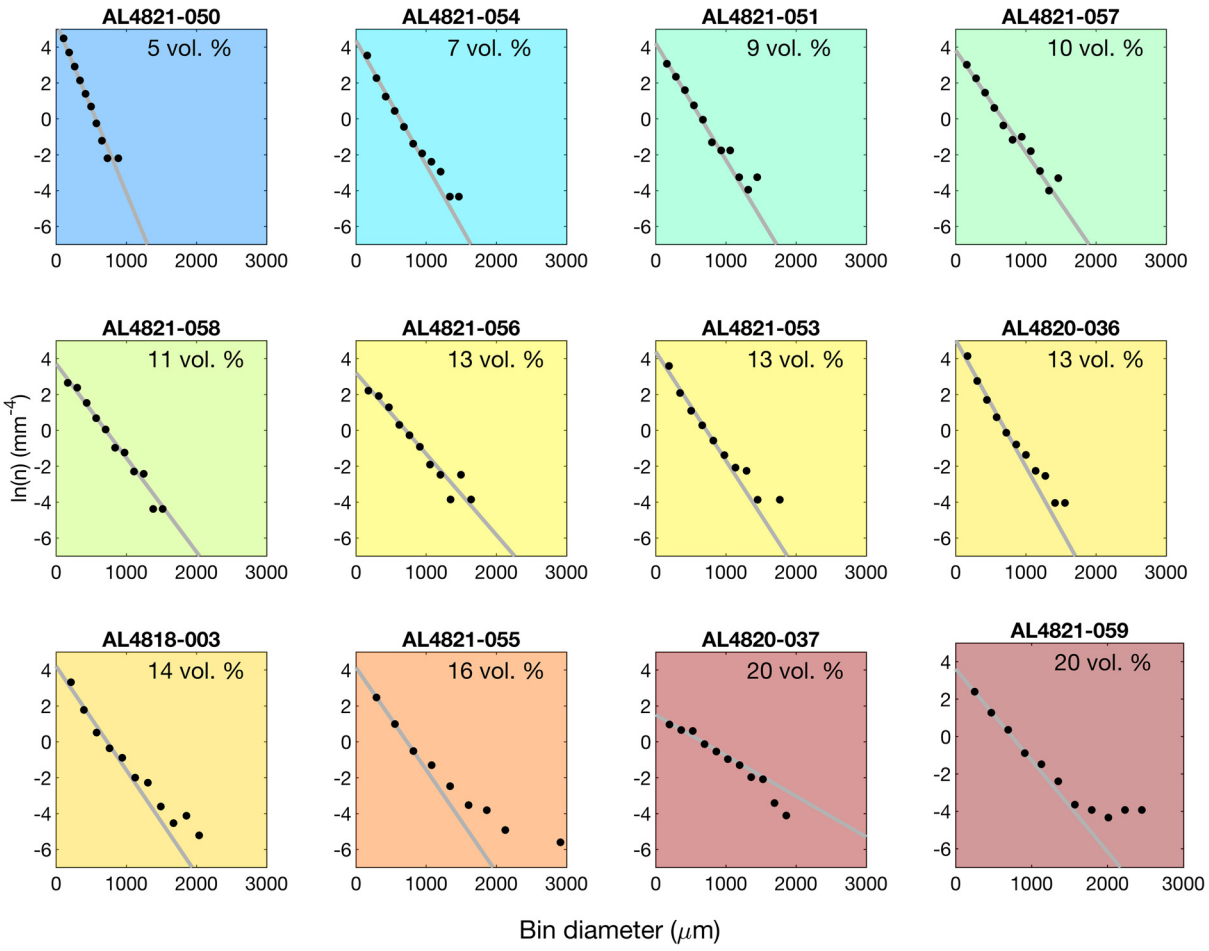

Fig. 6. Vesicle size distributions, shown as the natural log of the volumetric number density of bubbles normalized to the width of the bin as a function of the bin diameter, for 12 newly recovered popping rocks based on x-ray microtomography scans. The vesicle size distributions from high vesicularity popping rocks (>10%) are often distinct relative to low vesicularity (5–7%) popping rocks, including more large bubbles (>1.5 mm diameter) than expected based on a simple bubble nucleation and growth model. Log–linear reference lines, based on least-squares regressions of ln(n) on size classes <1 mm, are shown in order to highlight deviations at large size classes in some high vesicularity samples.

locations along a pillow ridge. These geochemical similarities also suggest that the variable CO_2 contents cannot be explained by dilution during progressive mantle melting, enrichment during fractional crystallization, or magma mixing, because these processes would produce comparable systematics in trace elements that behave similarly to carbon (e.g., Nb, Ba, Rb). Thus, a subset of these samples must have experienced either gas accumulation or gas loss in order to produce variable CO_2 concentrations despite homogeneous trace element ratios and REE patterns.

Vesicle size distributions and $^4He/^{40}Ar^*$ are influenced by gas accumulation and gas loss, and thus have the potential to provide insight into the processes controlling volatile concentrations in popping rocks (Cashman and Mangan, 1994; Marty and Tolstikhin, 1998; Moreira and Kurz, 2013; Sarda and Graham, 1990; Tucker et al., 2018). Progressive equilibrium degassing (i.e., gas loss from the magma) would be expected to produce enriched $^4He/^{40}Ar^*$ ratios in the lowest vesicularity samples due to the greater solubility of ^4He relative to ^{40}Ar (Burnard et al., 2004; Paonita and Martelli, 2007; Sarda and Moreira, 2002). However, the newly recovered popping rocks display consistently low $^4He/^{40}Ar^*$ ratios relative to the mantle production ratio (Marty and Tolstikhin, 1998) (Fig. 7), which indicates that the variable volatile concentrations in these samples does not reflect open-system, equilibrium (i.e., solubility controlled) degassing (Moreira and Kurz, 2013). Disequilibrium (i.e., diffusion controlled) degassing can fractionate noble gases in the opposite sense due to the lower diffusivity of ^{40}Ar relative to ^4He, which counteracts the lower solubility of ^{40}Ar. In the case of instantaneous, continuous gas loss (i.e., Rayleigh distillation), disequilibrium degassing would still produce slightly elevated $^4He/^{40}Ar^*$ ratios in samples with 20–50% of the initial gas content retained based on the average degree of disequilibrium necessary to produce MORB noble gas systematics (Tucker et al., 2018). Although discrete episodes of syn-eruptive, open-system, disequilibrium gas loss could produce low $^4He/^{40}Ar^*$ ratios in degassed samples (Gonnermann and Mukhopadhyay, 2007), shallow disequilibrium degassing would also likely produce dissolved CO_2 concentrations greater than experimentally determined solubilities at the eruption depths based on similar C and Ar diffusivities (Paonita and Martelli, 2006), which is not observed in the newly recovered popping rocks. There are uncertainties in the mantle $^4He/^{40}Ar^*$ production ratio, related to K, U, and Th abundances and mantle residence time, which hinders interpretation of the small difference between the new popping rocks data presented here and the putative mantle production ratio of 3 ± 1 (Marty and Tolstikhin, 1998). Our results show that the popping rocks have consistently low $^4He/^{40}Ar^*$ despite highly variable total volatile concentrations. These results are consistent with a bubble accumulation model, but could potentially reflect more complex degassing, such as discrete multi-stage episodes of gas loss and addition at various pressures.

Vesicle size distributions in erupted basalts also provide insight into magma storage and transport histories because volatile exsolution (i.e., bubble formation and growth) depends on depressurization rates and timescales (Cashman and Mangan, 1994). Dur-

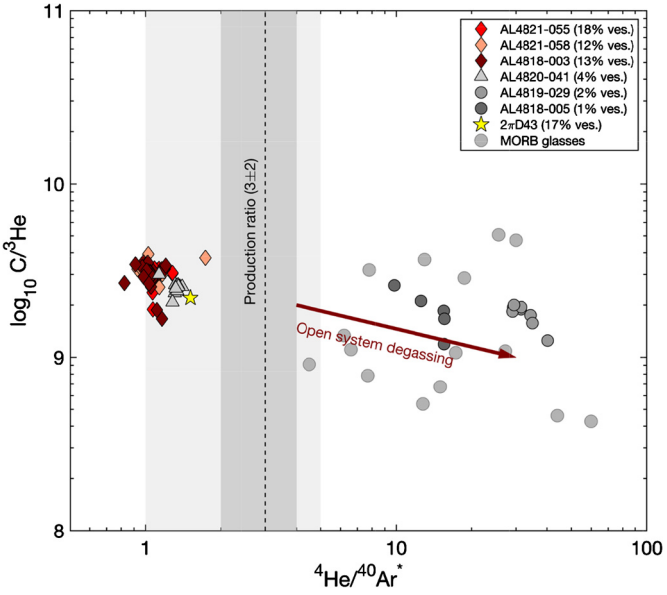

Fig. 7. $C/^3He$ vs. $^4He/^{40}Ar^*$ for three popping rock samples (diamonds), one geochemically similar, non-popping sample (AL4820-041), and two geochemically distinct samples (AL4818-005 and AL4819-029) relative to typical MORB (Marty and Tolstikhin, 1998). The popping rocks and proximal, geochemically similar non-popping rock (AL4820-041) display $^4He/^{40}Ar$ ratios similar to the mantle production ratio of 3 ± 1 (grey bar; Marty and Tolstikhin, 1998), demonstrating that gas loss did not produce the variable volatile concentrations in these samples. Data sources: 2πD43 popping rock: Moreira et al. (1998); MORB glasses: Marty and Tolstikhin (1998).

ing steady ascent from depth, magmas are expected to experience continuous vesicle nucleation and growth, leading to linear relationships between the natural log of the number of vesicles per unit volume (N_v) and the binned vesicle size (Sarda and Graham, 1990). The non-linear vesicle size distributions in high vesicularity popping rocks, marked by increased vesicle densities in the largest size classes, are likely caused by coalescence and/or accumulation (Chavrit et al., 2014; Sarda and Graham, 1990; Shea et al., 2010) (Fig. 5; Fig. 6). Although the x-ray μ-CT scans and reflected light photomicrographs show active bubble coalescence in the high vesicularity popping rocks (e.g., Fig. 5), coalescence alone cannot explain both the vesicle size distributions and the highly variable volatile concentrations (Fig. 1; Figs. 5–6; Table 1). Therefore, we suggest that bubble accumulation also influenced a subset of the popping rocks. Bubble accumulation was previously suggested for popping rock 2πD43 based on an empirical model for primary CO_2 concentrations derived from K_2O/TiO_2 ratios, axial valley depths, and spreading rates (Chavrit et al., 2014). Although some amount of degassing may still have affected the lowest vesicularity samples, the $^4He/^{40}Ar^*$ ratios, vesicle size distributions, and variable total volatile concentrations in these samples are consistent with gas accumulation as the mechanism to produce high vesicularity popping rocks at 13°46′N on the MAR. Our interpretation that gas accumulation influences the volatile concentrations in popping rocks implies that these samples may not reflect primary mantle-derived carbon concentrations.

4.2. Mechanisms for popping rock formation

Degassing during magma storage and transport affects volatile concentrations in most MORB based on total glass CO_2 concentrations consistent with equilibration at pressures associated with known magma storage reservoirs (e.g., Jones et al., 2018; Soule et al., 2012), greater CO_2 abundances in phenocryst hosted melt inclusions than in the carrier magmas (e.g., Helo et al., 2011), and higher $^4He/^{40}Ar^*$ in vesicles than predicted from the mantle production ratio (e.g., Marty and Tolstikhin, 1998). Only a few high-vesicularity popping rocks have been recovered from the global MOR system (e.g., 36°N MAR (Hekinian et al., 1973), Equatorial MAR (Le Voyer et al., 2015), Mathematician Ridge on the East Pacific Rise (Batiza and Vanko, 1985)), which shows that processes leading to gas accumulation are atypical. We hypothesize that the Popping Rock Ridge samples experienced gas accumulation during storage at crustal depths (Fig. 8). Magma storage within a compressional regime associated with bending of the 13°48′N OCC subsurface footwall (e.g., Parnell-Turner et al., 2017) may have prevented gas loss through the top of the magma reservoir and facilitated the accumulation of volatiles contained within the reservoir. Other mechanisms to decrease the permeability of the magma reservoir boundaries are also possible, including increasing lithospheric pressure with greater depths of storage (Fig. 8).

4.3. Implications for undegassed MORB and mantle carbon estimates

Volatile accumulation increases CO_2 concentrations relative to similarly incompatible elements. Based on the interpretation that the unusually high volatile concentrations in popping rocks reflects bubble accumulation, the highest CO_2/Nb or CO_2/Ba ratio from the Popping Rock Ridge samples does not represent a primitive, undegassed magma. Although it is difficult to constrain the pre-accumulation volatile concentration, we suggest that intermediate vesicularity samples from Popping Rock Ridge (5–7 vol.%; 2,450–3,450 ppm CO_2) provide the closest approximation based on their simple, log–linear vesicle size distributions (Fig. 5; Fig. 6) and $^4He/^{40}Ar^*$ ratios near the production ratio (e.g., 1.31 ± 0.06; Fig. 7). Our estimated pre-accumulation vesicularity and CO_2 concentration agrees with predictions from an empirical model derived from global K_2O/TiO_2 ratios, spreading rates, and axial valley depths (Chavrit et al., 2014). Popping rocks with 5–7% vesicularity have lower CO_2/Nb (98–137) and CO_2/Ba (16–22) ratios than all previous estimates for undegassed melts (Le Voyer et al., 2015; Michael and Graham, 2015; Saal et al., 2002) except three undersaturated MORB glasses from Gakkel Ridge in the Arctic Ocean (Michael and Graham, 2015). While it is possible that complex degassing processes influenced the intermediate vesicularity popping rocks without affecting $^4He/^{40}Ar^*$ ratios or vesicle size distributions, we explore the implications of the simple bubble accumulation model, in which popping rocks with 5–7% vesicularity reflect primary volatile concentrations, for carbon concentrations in the upper mantle and ridge CO_2 flux.

The inferred pre-accumulation volatile concentration in popping rocks implies that there are large heterogeneities in the CO_2/incompatible trace element ratio of the depleted MORB mantle (DMM). Further, CO_2/Ba and CO_2/Nb ratios from pre-accumulation popping rocks are less than ratios in most undegassed ultra-depleted and depleted MORB (Fig. 1; Le Voyer et al., 2017; Michael and Graham, 2015; Saal et al., 2002), and indicate that these ratios do not scale with trace element enrichment. The lack of a positive correlation between incompatible trace element and CO_2 enrichment in DMM implies that mantle carbon concentrations are lower and less heterogeneous than inferred from the post-accumulation CO_2/Nb ratio (556) of popping rock 2πD43, which has been used to suggest that mantle carbon concentrations vary by almost two orders of magnitude globally (Le Voyer et al., 2017). In addition, heterogeneities in primary CO_2/incompatible trace element ratios indicate that annual ridge CO_2 flux cannot necessarily be accurately calculated using a single CO_2/Nb or CO_2/Ba ratio, the estimated DMM Nb or Ba concentration, and the estimated annual volume of basaltic magma produced along the MOR system. These implications are based on the interpretation that gas accumulation produced the high-vesicularity popping rocks and that intermediate vesicularity samples reflect primary volatile concen-

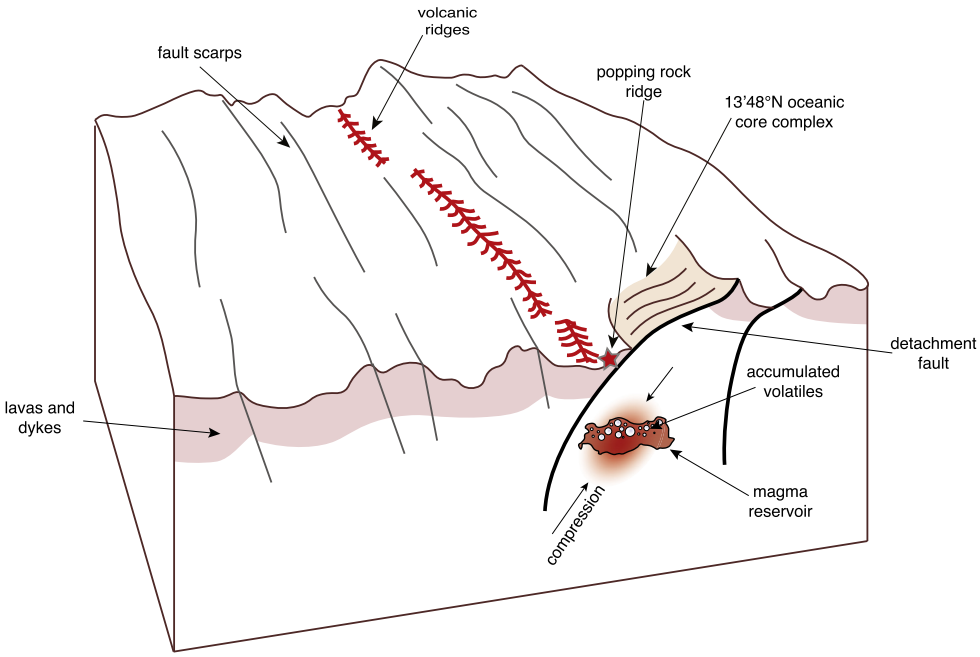

Fig. 8. Schematic representation showing the geologic setting and a possible formation mechanism for popping rocks near 13°46′N. Seafloor features are based on bathymetry presented in Smith et al. (2008) and the ridge structure is adapted from Escartin and Canales (2011). The popping rocks were found ~7 km west of the 13°48′N OCC, near the boundary between 'tectonic' and 'magmatic' ridge segments. The volatile concentrations, major and trace element geochemistry, and noble gas geochemistry in these samples are consistent with bubble accumulation as a formation mechanism. In contrast to 'typical' MORB, popping rocks may have experienced volatile accumulation rather than loss due to storage within a compressional regime associated with the 13°48′N OCC (e.g., Parnell-Turner et al., 2017) or the sealing of cracks that would typically allow gas loss due to storage at high-pressures.

trations. If the vesicle size distributions, low $^{4}He/^{40}Ar^{*}$ ratios, and highly variable volatile concentrations instead reflect extreme degrees of disequilibrium during degassing, the highest vesicularity samples could reflect primary volatile concentrations, indicating primary $CO_2/Nb = 500–650$ for popping rocks (Table 1) and large variability in mantle carbon concentrations (e.g., Le Voyer et al., 2017). Multiple discrete episodes of gas loss and addition could potentially produce these observations, which would complicate the interpretation of mantle volatile concentrations based on popping rocks because the primary concentration would likely not correspond with either the highest or lowest vesicularity.

5. Conclusions

Carbon strongly influences the viscosity and oxidation state of the mantle, melt formation and migration, long-term climate cycling, and volcanic processes. Rare, undegassed MORB and melt inclusions provide important constraints on the carbon content of the upper mantle. A suite of newly recovered *in situ* popping rocks from the Mid-Atlantic Ridge near 14°N contain highly variable vesicularities (5–24 vol.%) and total volatile concentrations (3,100–16,200 ppm CO_2) despite relatively homogeneous major and trace element geochemistry (e.g., $[La/Sm]_N = 1.76–1.84$) and consistently low $^{4}He/^{40}Ar^{*}$ ratios (1.05–1.09). Vesicle size distributions are log–linear with slight deviations in large size classes in the highest vesicularity samples, possibly reflecting coalescence or accumulation. Bubble accumulation is consistent with all of our observations, whereas coalescence can explain the deviations observed in the vesicle size distributions but not the variable total volatile concentrations. We suggest that popping rocks, which are the only volatile-saturated MORB previously inferred to represent 'undegassed' magmas, are not representative of primary mantle volatile concentrations and are instead influenced by gas accumulation. The results imply lower CO_2/Nb or CO_2/Ba than previously inferred based on undegassed MORB and lower and less heterogeneous mantle carbon concentrations.

Author contributions

All authors contributed to interpretation and writing. MRJ, SAS, MDK, and HB contributed volatile measurements. MRJ and HB measured vesicularity characteristics. MRJ and FK contributed Raman measurements. MDK and JC measured noble gases. VDW contributed major and trace element measurements. MRJ, VDW, SAS, MDK, EM, DJF, JC, FK, SP, and DMS contributed to sample collection.

Acknowledgements

We gratefully acknowledge the captain, operations teams, marine technicians, and crew of the *R/V Atlantis*, the operations teams of the *AUV Sentry* and *HOV Alvin*, and the entire scientific party onboard AT33-03. We appreciate the analytical assistance provided by B. Monteleone, S. Bendana, and M. Lytle. We thank M. Hirschmann and an anonymous reviewer for insightful comments on an earlier version of this manuscript and T. Mather for editorial handling. Seagoing and analytical efforts were supported by National Science Foundation grants OCE-1259218 and OCE-1260578 to M. Kurz and E. Mittelstaedt. M. Jones acknowledges support provided by the Department of Defense (DoD) through the National Defense Science & Engineering Graduate Fellowship (NDSEG) Program.

Appendix A. Supplementary material

Supplementary material related to this article can be found online at https://doi.org/10.1016/j.epsl.2019.01.019.

References

Aster, E.M., Wallace, P.J., Moore, L.R., Watkins, J., Gazel, E., Bodnar, R.J., 2016. Reconstructing CO_2 concentrations in basaltic melt inclusions using Raman analysis of vapor bubbles. J. Volcanol. Geotherm. Res. 323, 148–162. https://doi.org/10.1016/j.jvolgeores.2016.04.028.

Batiza, R., Vanko, D.A., 1985. Petrologic evolution of large failed rifts in the Eastern Pacific: petrology of volcanic and plutonic rocks from the mathematician ridge area and the Guadalupe trough. J. Petrol. 26, 564–602. https://doi.org/10.1093/petrology/26.3.564.

Bougault, H., Dmitriev, L., Schilling, J.G., Sobolev, A., Joron, J.L., Needham, H.D., 1988. Mantle heterogeneity from trace elements: MAR triple junction near 14°N. Earth Planet. Sci. Lett. 88, 27–36. https://doi.org/10.1016/0012-821X(88)90043-X.

Burnard, P., 1997. Vesicle-specific noble gas analyses of "popping rock": implications for primordial noble gases in Earth. Science 276, 568–571. https://doi.org/10.1126/science.276.5312.568.

Burnard, P., Graham, D., Farley, K., 2004. Fractionation of noble gases (He, Ar) during MORB mantle melting: a case study on the Southeast Indian Ridge. Earth Planet. Sci. Lett. 227, 457–472. https://doi.org/10.1016/j.epsl.2004.08.021.

Burnard, P., Reisberg, L., Colin, A., 2014. An observed link between lithophile compositions and degassing of volatiles (He, Ar, CO_2) in MORBs with implications for Re volatility and the mantle C/Nb ratio. Earth Planet. Sci. Lett. 395, 159–167. https://doi.org/10.1016/j.epsl.2014.03.045.

Cartigny, P., Pineau, F., Aubaud, C., Javoy, M., 2008. Towards a consistent mantle carbon flux estimate: insights from volatile systematics (H_2O/Ce, δD, CO_2/Nb) in the North Atlantic mantle (14°N and 34°N). Earth Planet. Sci. Lett. 265, 672–685. https://doi.org/10.1016/j.epsl.2007.11.011.

Cashman, K.V., Mangan, M.T., 1994. Physical aspects of magmatic degassing II. Rev. Mineral. Geochem. 30, 447–478.

Chavrit, D., Humler, E., Grasset, O., 2014. Mapping modern CO_2 fluxes and mantle carbon content all along the mid-ocean ridge system. Earth Planet. Sci. Lett. 387, 229–239. https://doi.org/10.1016/j.epsl.2013.11.036.

Dasgupta, R., Hirschmann, M.M., 2010. The deep carbon cycle and melting in Earth's interior. Earth Planet. Sci. Lett. 298, 1–13. https://doi.org/10.1016/j.epsl.2010.06.039.

Dasgupta, R., Mallik, A., Tsuno, K., Withers, A.C., Hirth, G., Hirschmann, M.M., 2013. Carbon-dioxide-rich silicate melt in the Earth's upper mantle. Nature 493, 211–215. https://doi.org/10.1038/nature11731.

Escartín, J., Canales, J.P., 2011. Detachments in oceanic lithosphere: deformation, magmatism, fluid flow, and ecosystems. Eos Trans. AGU 92, 31. https://doi.org/10.1029/2011EO040003.

Esposito, R., Bodnar, R.J., Danyushevsky, L.V., De Vivo, B., Fedele, L., Hunter, J., Lima, A., Shimizu, N., 2011. Volatile evolution of magma associated with the Solchiaro eruption in the Phlegrean Volcanic District (Italy). J. Petrol. 52, 2431–2460. https://doi.org/10.1093/petrology/egr051.

Gonnermann, H.M., Mukhopadhyay, S., 2007. Non-equilibrium degassing and a primordial source for helium in ocean-island volcanism. Nature 449, 1037–1040. https://doi.org/10.1038/nature06240.

Hauri, E., Wang, J., Dixon, J.E., King, P.L., Mandeville, C., Newman, S., 2002. SIMS analysis of volatiles in silicate glasses: 1. Calibration, matrix effects and comparisons with FTIR. In: Melt Inclusions at the Millennium: Toward a Deeper Understanding of Magmatic Processes. Chem. Geol. 183, 99–114. https://doi.org/10.1016/S0009-2541(01)00375-8.

Hekinian, R., Chaigneau, M., Cheminee, J.L., 1973. Popping rocks and lava tubes from the Mid-Atlantic Rift Valley at 36°N. Nature 245, 371–373. https://doi.org/10.1038/245371a0.

Helo, C., Longpre, M.-A., Shimizu, N., Clague, D.A., Stix, J., 2011. Explosive eruptions at mid-ocean ridges driven by CO_2-rich magmas. Nat. Geosci. 4, 260–263. https://doi.org/10.1038/NGEO1104.

Hirth, G., Kohlstedt, D.L., 1996. Water in the oceanic upper mantle: implications for rheology, melt extraction and the evolution of the lithosphere. Earth Planet. Sci. Lett. 144, 93–108. https://doi.org/10.1016/0012-821X(96)00154-9.

Huybers, P., Langmuir, C., 2009. Feedback between deglaciation, volcanism, and atmospheric CO_2. Earth Planet. Sci. Lett. 286, 479–491. https://doi.org/10.1016/j.epsl.2009.07.014.

Javoy, M., Pineau, F., 1991. The volatiles record of a "popping" rock from the Mid-Atlantic Ridge at 14°N: chemical and isotopic composition of gas trapped in the vesicles. Earth Planet. Sci. Lett. 107, 598–611.

Jones, M.R., Soule, S.A., Gonnermann, H.M., Le Roux, V., Clague, D.A., 2018. Magma ascent and lava flow emplacement rates during the 2011 Axial Seamount eruption based on CO_2 degassing. Earth Planet. Sci. Lett. 494, 32–41. https://doi.org/10.1016/j.epsl.2018.04.044.

Kurz, M.D., Curtice, J., Fornari, D., Geist, D., Moreira, M., 2009. Primitive neon from the center of the Galápagos hotspot. Earth Planet. Sci. Lett. 286, 23–34. https://doi.org/10.1016/j.epsl.2009.06.008.

Kurz, M.D., Moreira, M., Curtice, J., Lott III, D.E., Mahoney, J.J., Sinton, J.M., 2005. Correlated helium, neon, and melt production on the super-fast spreading East Pacific Rise near 17°S. Earth Planet. Sci. Lett. 232, 125–142. https://doi.org/10.1016/j.epsl.2005.01.005.

Lamadrid, H.M., Moore, L.R., Moncada, D., Rimstidt, J.D., Burruss, R.C., Bodnar, R.J., 2017. Reassessment of the Raman CO_2 densimeter. Chem. Geol. 450, 210–222. https://doi.org/10.1016/j.chemgeo.2016.12.034.

Le Voyer, M., Cottrell, E., Kelley, K.A., Brounce, M., Hauri, E.H., 2015. The effect of primary versus secondary processes on the volatile content of MORB glasses: an example from the equatorial Mid-Atlantic Ridge (5°N–3°S). J. Geophys. Res., Solid Earth 120, 125–144. https://doi.org/10.1002/2014JB011160.

Le Voyer, M., Kelley, K.A., Cottrell, E., Hauri, E.H., 2017. Heterogeneity in mantle carbon content from CO_2-undersaturated basalts. Nat. Commun. 8, 14062. https://doi.org/10.1038/ncomms14062.

Marty, B., Tolstikhin, I.N., 1998. CO_2 fluxes from mid-ocean ridges, arcs and plumes. Chem. Geol. 145, 233–248. https://doi.org/10.1016/S0009-2541(97)00145-9.

Matthews, S., Shorttle, O., Rudge, J.F., Maclennan, J., 2017. Constraining mantle carbon: CO_2-trace element systematics in basalts and the roles of magma mixing and degassing. Earth Planet. Sci. Lett. 480, 1–14. https://doi.org/10.1016/j.epsl.2017.09.047.

McDonough, W.F., Sun, S., 1995. The composition of the Earth. In: Chemical Evolution of the Mantle. Chem. Geol. 120, 223–253. https://doi.org/10.1016/0009-2541(94)00140-4.

Michael, P.J., Graham, D.W., 2015. The behavior and concentration of CO_2 in the suboceanic mantle: inferences from undegassed ocean ridge and ocean island basalts. Lithos 236–237, 338–351. https://doi.org/10.1016/j.lithos.2015.08.020.

Moore, L.R., Gazel, E., Tuohy, R., Lloyd, A.S., Esposito, R., Steele-MacInnis, M., Hauri, E.H., Wallace, P.J., Plank, T., Bodnar, R.J., 2015. Bubbles matter: an assessment of the contribution of vapor bubbles to melt inclusion volatile budgets. Am. Mineral. 100, 806–823. https://doi.org/10.2138/am-2015-5036.

Moreira, M., Kunz, J., Allegre, C., 1998. Rare gas systematics in popping rock: isotopic and elemental compositions in the upper mantle. Science 279, 1178–1181. https://doi.org/10.1126/science.279.5354.1178.

Moreira, M.A., Kurz, M.D., 2013. Noble gases as tracers of mantle processes and magmatic degassing. In: The Noble Gases as Geochemical Tracers, Advances in Isotope Geochemistry. Springer, Berlin, Heidelberg, pp. 371–391.

Paonita, A., Martelli, M., 2007. A new view of the He–Ar–CO_2 degassing at mid-ocean ridges: homogeneous composition of magmas from the upper mantle. Geochim. Cosmochim. Acta 71, 1747–1763. https://doi.org/10.1016/j.gca.2006.12.019.

Paonita, A., Martelli, M., 2006. Magma dynamics at mid-ocean ridges by noble gas kinetic fractionation: assessment of magmatic ascent rates. Earth Planet. Sci. Lett. 241, 138–158. https://doi.org/10.1016/j.epsl.2005.10.018.

Parnell-Turner, R., Sohn, R.A., Peirce, C., Reston, T.J., MacLeod, C.J., Searle, R.C., Simão, N.M., 2017. Oceanic detachment faults generate compression in extension. Geology 45, 923–926. https://doi.org/10.1130/G39232.1.

Perfit, M., Wanless, V.D., Ridley, W.I., Klein, E., Smith, M., Goss, A., Hinds, J., Kutza, S., Fornari, D., 2012. Lava geochemistry as a probe into crustal formation at the East Pacific Rise. Oceanography 25, 89–93. https://doi.org/10.5670/oceanog.2012.06.

Rosenthal, A., Hauri, E.H., Hirschmann, M.M., 2015. Experimental determination of C, F, and H partitioning between mantle minerals and carbonated basalt, CO_2/Ba and CO_2/Nb systematics of partial melting, and the CO_2 contents of basaltic source regions. Earth Planet. Sci. Lett. 412, 77–87. https://doi.org/10.1016/j.epsl.2014.11.044.

Saal, A.E., Hauri, E.H., Langmuir, C.H., Perfit, M.R., 2002. Vapour undersaturation in primitive mid-ocean-ridge basalt and the volatile content of Earth's upper mantle. Nature 419, 451–455. https://doi.org/10.1038/nature01073.

Sarda, P., Graham, D., 1990. Mid-ocean ridge popping rocks: implications for degassing at ridge crests. Earth Planet. Sci. Lett. 97, 268–289. https://doi.org/10.1016/0012-821X(90)90047-2.

Sarda, P., Moreira, M., 2002. Vesiculation and vesicle loss in mid-ocean ridge basalt glasses: He, Ne, Ar elemental fractionation and pressure influence. Geochim. Cosmochim. Acta 66, 1449–1458. https://doi.org/10.1016/S0016-7037(01)00863-8.

Schwartz, D.M., Wanless, V.D., Berg, R., Jones, M., Fornari, D.J., Soule, S.A., Lytle, M.L., Carey, S., 2017. Petrogenesis of alkalic seamounts on the Galápagos Platform. Deep-Sea Res., Part 2, Top. Stud. Oceanogr. https://doi.org/10.1016/j.dsr2.2017.09.019.

Shea, T., Houghton, B.F., Gurioli, L., Cashman, K.V., Hammer, J.E., Hobden, B.J., 2010. Textural studies of vesicles in volcanic rocks: an integrated methodology. J. Volcanol. Geotherm. Res. 190, 271–289. https://doi.org/10.1016/j.jvolgeores.2009.12.003.

Smith, D.K., Escartín, J., Schouten, H., Cann, J.R., 2008. Fault rotation and core complex formation: significant processes in seafloor formation at slow-spreading mid-ocean ridges (Mid-Atlantic Ridge, 13°–15°N). Geochem. Geophys. Geosyst. 9. https://doi.org/10.1029/2007GC001699.

Soule, S.A., Nakata, D.S., Fornari, D.J., Fundis, A.T., Perfit, M.R., Kurz, M.D., 2012. CO_2 variability in mid-ocean ridge basalts from syn-emplacement degassing: constraints on eruption dynamics. Earth Planet. Sci. Lett. 327–328, 39–49. https://doi.org/10.1016/j.epsl.2012.01.034.

Tucker, J.M., Mukhopadhyay, S., Gonnermann, H.M., 2018. Reconstructing mantle carbon and noble gas contents from degassed mid-ocean ridge basalts. Earth Planet. Sci. Lett. 496, 108–119. https://doi.org/10.1016/j.epsl.2018.05.024.

Wallace, P.J., Plank, T., Edmonds, M., Hauri, E.H., 2015. Volatiles in magmas. In: Sigurdsson, H. (Ed.), The Encyclopedia of Volcanoes, second edition. Academic Press, Amsterdam, pp. 163–183.

Wright, R.B., Wang, C.H., 1973. Density effect on the Fermi resonance in gaseous CO_2 by Raman scattering. J. Chem. Phys. 58, 2893–2895. https://doi.org/10.1063/1.1679594.